Binding of O_2 and Its Reduction Are Both Retarded by Replacement of Valine 279 by Isoleucine in Cytochrome *c* Oxidase from *Paracoccus denitrificans*†

Sirpa Riistama, Anne Puustinen, Michael I. Verkhovsky, Joel E. Morgan, and Mårten Wikström*

Helsinki Bioenergetics Group, Department of Medical Chemistry, Institute for Biomedical Sciences and Biocentrum Helsinki, P.O. Box 8 (Siltavuorenpenger 10A), FIN-00014 University of Helsinki, Finland

Received January 20, 2000; Revised Manuscript Received March 9, 2000

ABSTRACT: The crystal structure of the heme−copper oxidases suggested a putative channel of oxygen entry into the heme−copper site of O_2 reduction. Changing a conserved valine near this center in cytochrome bo_3 of *Escherichia coli* to isoleucine caused a significant increase in the apparent K_M for oxygen with little or no change in V_{max}, suggesting that oxygen diffusion had been partially blocked [Riistama, S., Puustinen, A., García-Horsman, A., Iwata, S., Michel, H., and Wikström, M. (1996) *Biochim. Biophys. Acta 1275*, 1−4]. To study this phenotype further using rapid kinetic methods, the corresponding change (V279I) has been made in cytochrome aa_3 from *Paracoccus denitrificans*. In this mutant, the apparent K_M for oxygen is 8 times higher than in the wild-type enzyme, whereas V_{max} is decreased only to approximately half of the wild-type value. Flow-flash kinetic measurements show that the initial binding of oxygen to the heme of the binuclear site is indeed much slower in the mutant than in the wild-type enzyme. However, the subsequent phases of the reaction with O_2 are also slow although the pure heme-to-heme electron transfer process is essentially unperturbed. It is suggested that the mutation sterically hinders O_2 entry into the binuclear site and that it may also perturb the structure of local water molecules involved in proton transfer to this site.

Consumption of oxygen plays a key role in the process by which most living cells obtain energy from their surroudings. Reduction of dioxygen to water serves, in effect, as the positive pole of a battery. Electrons which are derived from the oxidation of foodstuffs flow to this pole via a series of membrane-bound enzymes known collectively as the respiratory chain. The enzymes which make up the chain draw energy from this current to create and maintain an electrochemical proton gradient ($\Delta\mu_{H+}$)[1] across the membrane. This gradient is the source of energy for the synthesis of ATP.

The final element in the respiratory chain, where reduction of oxygen to water actually takes place, is known as the terminal oxidase. In eukaryotic organisms this role is played by cytochrome *c* oxidase, which resides in the mitochondrial inner membrane along with the other members of the respiratory chain (*1*). This enzyme, and its bacterial relatives, make up an enzyme family known as the heme−copper oxidases, which transduce redox energy energy into $\Delta\mu_{H+}$ by two mechanisms: The reduction of oxygen is arranged topographically in such a way that the electrons and protons needed to make water are obtained from opposite sides of the membrane, making the redox reaction itself electrogenic. In addition, the reaction drives a proton-pumping function, effectively doubling the amount of energy conserved (*1*, *2*).

In almost all cytochrome *c* oxidases, electrons enter the enzyme at Cu_A, a binuclear copper center—but a one electron carrier—near the membrane surface. From Cu_A, electrons flow to a low-spin heme site (heme *a* or Fe_a) and from there to a binuclear heme−copper site (heme a_3−Cu_B) where the actual reduction of dioxygen takes place. The low-spin heme is close to the dioxygen-binding heme, and structural models show the two hemes buried to roughly the same depth in the membrane (*3*−*5*). These crystal structure models of cytochrome *c* oxidase revealed what appeared to be a hydrophobic channel by which O_2 could reach the binuclear site of the enzyme from the hydrophobic core of the membrane (*6*). To study this further, a series of mutations were constructed in the closely related enzyme, cytochrome bo_3 of *Escherichia coli*, with the intention of sterically blocking oxygen diffusion through this putative channel. One of these mutants, in which a conserved valine close to the oxygen reduction site was replaced by isoleucine (V287I in the *E. coli* sequence numbering), showed a markedly lower apparent affinity for oxygen with little or no effect on V_{max} (*6*), suggesting restriction of oxygen diffusion into the enzyme and pointing to a likely oxygen diffusion path. The same path was also indicated by molecular dynamics calculations of O_2 diffusion in the X-ray structure model (*7*). However, direct demonstration of restricted oxygen entry requires kinetic resolution of the initial formation of the ferrous−oxy intermediate.

Kinetic and spectroscopic studies have resolved a number of steps in the reaction of cytochrome *c* oxidase with

† This work was supported by grants from The Academy of Finland, The University of Helsinki, the Sigrid Jusélius Foundation, and Biocentrum Helsinki.

* To whom correspondence should be sent. E-mail: Marten.Wikstrom@Helsinki.Fi.

[1] Abbreviations: **A**, the ferrous−oxy compound of Fe_{a3}; DM, dodecyl maltoside; $\Delta\mu_{H+}$, electrochemical membrane proton gradient; **F**, ferryl intermediate; Fe_a, low-spin heme; Fe_{a3}, the oxygen binding heme; **O**, fully oxidized form of binuclear oxygen reduction site; **P**, "peroxy" intermediate; PMSF, phenylmethylsulfonyl fluoride; **R**, unliganded, fully reduced enzyme; τ, time constant ($t_{1/e}$); TMPD, *N*,*N*,*N*′,*N*′-tetramethyl-1,4-phenylenediamine.

10.1021/bi000123w CCC: $19.00
Published on Web 05/04/2000

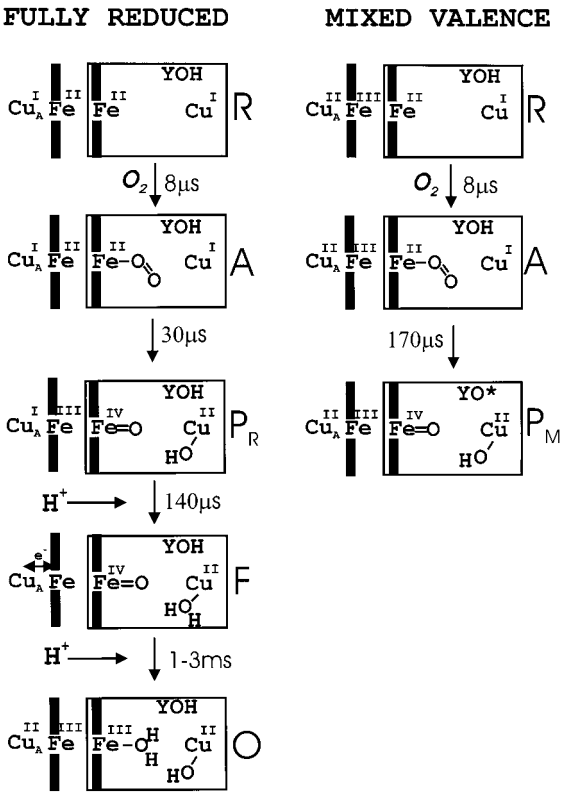

FIGURE 1: Reaction of cytochrome *c* oxidase with O_2. The boxes and the symbols represent states of the binuclear heme a_3−Cu_B oxygen reduction site, which includes the conserved tyrosine 280 (YOH). The proximal ligand of heme a_3 and an oxygenous ligand of Cu_B are shown. The Cu_A center and the low-spin heme *a* are depicted on the left of the box. In state F one electron is shared between heme *a* and Cu_A. The sequence on the left depicts the reaction of the fully reduced enzyme with O_2. On the right, the reaction of the two-electron reduced, "mixed valence", enzyme is shown. YO* denotes the neutral tyrosine 280 radical. Approximate time constants at RT for the individual reaction steps are given. The initial reaction with dioxygen shows the time constant at 1 mM O_2.

oxygen: When the oxygen molecule first enters the enzyme, it is believed to bind weakly to Cu_B (*8*, *9*), the copper ion of the heme−copper site, and subsequently to Fe_{a3} to form a ferrous−oxy compound (**A**), the first spectroscopically identifiable intermediate in the reaction (Figure 1). Perhaps surprisingly for an enzyme whose function is to consume oxygen, the initial binding of O_2 in the ferrous−oxy species is very weak (*10*, *11*). Instead of acquiring the oxygen molecule by tight binding—an energetically expensive alternative—the enzyme makes a rapid but loose attachment, and the O_2 molecule is subsequently "trapped" by the first redox step of the reaction. This achieves an apparent dioxygen affinity for the enzyme's reaction which is orders of magnitude more favorable than the binding affinity itself (*10*, *11*).

The step in which O_2 is trapped ($\tau \sim 30$ μs) converts the ferrous−oxy intermediate (**A**) into intermediate **P**, so named because it was originally thought to be a peroxy species (*12*). In the reaction of the fully reduced enzyme with O_2, the low-spin heme becomes oxidized at the same time that **P** is formed (*13*−*16*; Figure 1, left). In fact, the rate of the oxygen-trapping reaction depends critically on how quickly the electron from the low-spin heme can arrive at the binuclear center. Experiments with a variant form of cytochrome bo_3 from *E. coli* in which the heme-to-heme electron transfer is slow (*17*) showed a corresponding decrease in the rate of this initial redox step of the oxygen reaction (*9*, *18*, *19*).

The reaction with dioxygen can also be initiated from a "mixed-valence" state in which only Fe_{a3} and Cu_B are reduced, so that no electron transfer is possible from the low-spin heme. Now oxygen is still trapped but at a five times slower rate. While the ferrous−oxy compound (**A**) forms normally, the subsequent conversion of **A** to **P** is slow ($\tau \sim$ 170 μs; *20*). Here, the **P** intermediate forms with one less reducing equivalent in the heme−copper site and has been named $\mathbf{P}_M$ (Figure 1, right). The **P** intermediate, which forms simultaneously with oxidation of the low-spin heme, has been named $\mathbf{P}_R$. Both $\mathbf{P}_M$ and $\mathbf{P}_R$ have the same characteristic 607 nm absorbance, so it seems likely that the iron−oxygen moiety is the same in both cases (*21*). The consensus today, on the basis of spectroscopic data, is that both species have an oxoferryl iron at Fe_{a3} (*22*−*26*). The additional oxidizing equivalent in $\mathbf{P}_M$ is probably a neutral radical of an invariant tyrosine residue that is covalently linked to a histidine Cu_B ligand (*27*−*29*; Figure 1), although a trivalent Cu_B state cannot be excluded.

When the $\mathbf{P}_R$ intermediate is reached in the reaction of the fully reduced enzyme with oxygen, Fe_a is oxidized and the fourth electron is still on Cu_A. In the next phase ($\tau \sim$ 140 μs at RT (room temperature); *20*), $\mathbf{P}_R$ is converted to the oxy−ferryl species **F** (*30*−*32*). At approximately the same time, Cu_A becomes partially oxidized as the fourth electron equilibrates between Cu_A and Fe_a (*15*), as indicated in Figure 1 (left). Finally, in a much slower process ($\tau \sim$ 1−3 ms), the remaining electron, shared between Fe_a and Cu_A, migrates to the binuclear center resulting in the conversion of **F** into the fully oxidized enzyme, **O** (*15*). Clearly, kinetic studies of this type, which can resolve the initial formation of the ferrous−oxy intermediate **A**, were needed to clarify the nature of the inhibition in the V287I mutant. However, cytochrome bo_3 is a poor vehicle for this type of measurements as compared to cytochrome aa_3 (*33*). We have therefore constructed the corresponding mutant in the cytochrome aa_3 of *Paracoccus denitrificans*, viz. V279I.[2] Here, using this new mutant enzyme, we report the kinetic consequences of the mutation in some depth. As expected, the binding of oxygen to form the ferrous−oxy intermediate **A** is considerably decelerated. Surprisingly, however, subsequent reaction steps also proceed at significantly slower rates than in the wild-type enzyme.

MATERIALS AND METHODS

Site-Directed Mutagenesis. The system used for in vitro mutagenesis was based on the method of Vandeyar et al. (*34*). A 1.6 kB Pst I−Hind III fragment containing the *ctaDII* gene which encodes subunit I of *P. denitrificans* cytochrome aa_3 (*35*) was moved into M13mp18 and used as a template. After mutagenesis, the mutant gene was cloned into a derivative of the broad host range plasmid pEG400 (*36*) containing a streptomycin marker and the *ctaDII* gene, together with its promotor region. The *E. coli* strain SM10 transformed with this plasmid was conjugated with *P.*

[2] Unless otherwise noted, amino acid sequence numbering refers to subunit I of cytochrome *c* oxidase from *P. denitrificans*.

denitrificans strain 9220, from which the chromosomal copies of the *ctaDII* and its isogene *ctaDI* had been deleted (*37*). The mutation was confirmed by DNA sequencing (ALFexpress DNA sequencer, Pharmacia) throughout all processing states, as well as from fermentor cultivations.

Bacterial Growth and Enzyme Purification. Wild-type and mutant strains of *P. denitrificans* were grown at 32 °C under strong aeration in a fermentor using succinate (50 mM) as carbon source in minimal medium (*38*) that was supplemented by streptomycin (25 μg/mL). Cells were harvested in the exponential growth phase, and the enzyme was isolated as described earlier (*39*).

Activity Measurements. Oxygen consumption was measured polarographically at 25 °C, using a Clark type oxygen electrode. The medium contained 50 mM KCl, 0.5 mM EDTA, and 50 mM Tris-Cl, pH 7.5, supplemented with 11 mM K^+ ascorbate, 24 μM horse heart cytochrome *c* (Sigma), 1.1 mM TMPD, and 0.3 mg/mL asolectin. The rate of oxygen uptake was determined after addition of the enzyme. To determine the apparent K_M for O_2, the reaction was allowed to continue until all the oxygen in the measuring cell was consumed.

Proton Translocation. Spheroplast treatment of the *P. denitrificans* cells and the oxidant pulse method to measure proton translocation were as described previously (*40*). The reaction medium contained either 100 mM KSCN, 100 mM KCl, 100 mM sucrose, and 3 mM $MgCl_2$ or 200 mM KCl, 100 mM sucrose, 3 mM $MgCl_2$, and 0.5−1 μM valinomycin, supplemented with 10−20 μM rotenone and 2.5 mM succinate.

Kinetic Measurements. Methods for room-temperature flow-flash (*9*), low-temperature flow-flash (*21*), and anaerobic photolysis (*17*) measurements have been published previously.

Data Analysis. Basic data matrix manipulations and presentation were done with MATLAB (The Mathworks, South Natick, MA). Decomposition of data surfaces was done using SPLMOD (*41*), a global multiexponential fitting program running under a MATLAB front-end interface.

FTIR Spectroscopy. Purified wild-type and V279I enzymes were diluted 10-fold into 100 mM sodium phosphate and 0.01% DM, pH 7.8, in D_2O and reconcentrated. This was repeated twice. Enzyme samples (0.2−0.3 mM) were made air-free by repeated vacuum/argon cycling and then reduced by dithionite, after which CO (1 mM) was mixed into the solution. Cells for IR spectroscopy had CaF_2 windows and 50 μm Teflon spacers. Spectra were recorded at either 230 or 278 K using a Bruker I55 spectrometer equipped with a modified Specac cryostat and a Lauda RK8-CS thermostat bath circulating ethanol. To obtain "light-minus-dark" spectra, data were acquired in sets of 64 scans, alternately with and without illumination of the sample. The results were subsequently averaged and subtracted. "Light" spectra were acquired under continuous off-axis illumination of the sample by a mercury arc lamp, the beam of which had been passed through a water filter and a Schott BG-3 filter. A 6 mm thick germanium plate was used to keep the photolysis light out of the MCT infrared detector.

RESULTS

After the V279I mutant of *P. denitrificans* cytochrome aa_3 had been expressed and purified, it was necessary to confirm that it had the same interesting steady-state turnover properties as the original cytochrome bo_3 mutant. Figure 2 shows the dependence of enzyme activity on oxygen concentration during steady-state turnover for wild-type *P. denitrificans* cytochrome aa_3 and the V279I mutant enzyme. The effect of the mutation on the apparent K_M for dioxygen is similar to that of the corresponding mutation in *E. coli* cytochrome bo_3. The apparent K_M for oxygen is 8 times higher whereas the V_{max} is decreased only by ca. 50%, as compared to the wild-type enzyme. The mutant enzyme was found to pump protons with the same efficiency as the wild type in multiturnover experiments with spheroplasts (not shown), as was the case for the *E. coli* mutant enzyme (*6*).

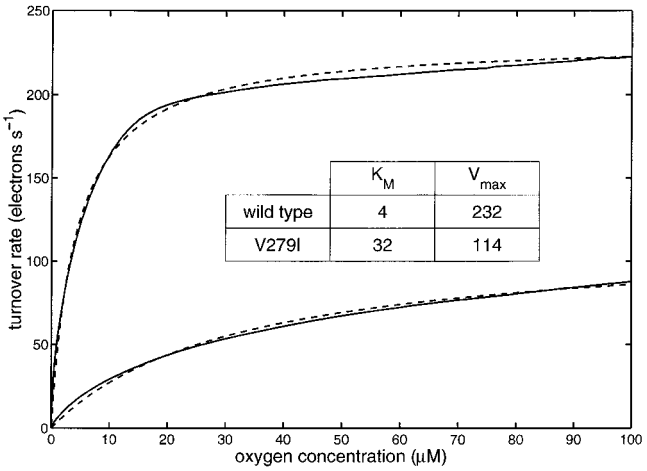

FIGURE 2: Oxygen concentration dependence of respiration in isolated wild-type cytochrome aa_3 (upper) and V279I mutant (lower) from *P. denitrificans*. O_2 consumption was measured polarographically at 25 °C. Key: Solid lines, experimental data; dashed lines, best fits with the indicated values for V_{max} and $K_{M,app}$.

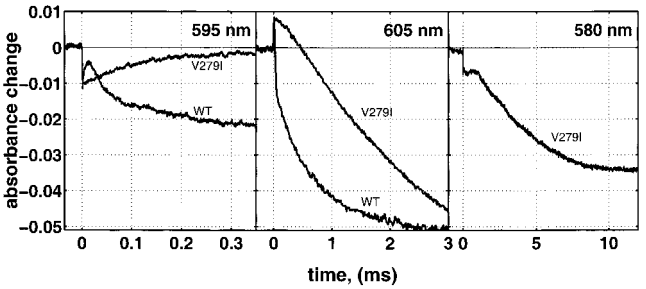

FIGURE 3: Flow-flash reaction of fully reduced wild type and V279I mutant cytochrome aa_3 from *P. denitrificans* with O_2. Zero on the time scale is the point at which the laser was fired. Concentrations after mixing: tricine, 100 mM (pH 8); DM, 0.025%; ascorbate, 0.4 mM; TMPD, 17 μM; enzyme, 2.5 μM; O_2, 1 mM.

Since the valine-to-isoleucine mutant in cytochrome aa_3 from *P. denitrificans* therefore also shows indications of hindered O_2 entry, we set out to observe the binding of oxygen directly. The kinetics of oxygen binding to the enzyme as well as the initial steps in the reduction of oxygen to water can be studied using the "flow-flash" method (*42*) in which the reduced enzyme, inhibited by carbon monoxide, is mixed with oxygen in the dark and the reaction initiated rapidly by photodissociating the bound CO. Figure 3 shows the time course of the oxygen reaction in wild-type and V279I mutant enzyme. The traces in the left panel show absorbance changes at 595 nm, the λ_{max} for the ferrous−oxy intermediate **A** in aa_3 type enzymes (*10, 33*). In the wild-type enzyme, photolysis of CO—the jump at time zero—is

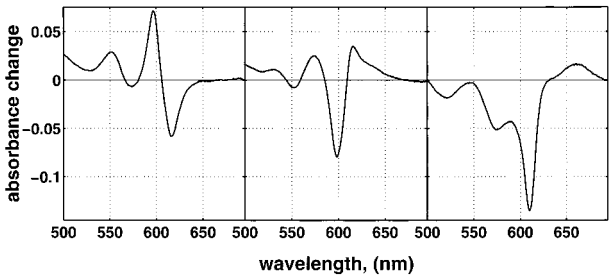

FIGURE 4: Kinetic component spectra from reactions of fully reduced V279I mutant cytochrome aa_3 from *P. denitrificans* with O_2 at low temperature (−20 °C): left panel, rate constant too fast to resolve accurately; center panel, $k = 84$ s^{-1}; right panel, $k = 28.8$ s^{-1}. Spectra were obtained by a four-component fit (see Materials and Methods) of which only the first three are shown; the small fourth component had a rate constant of 7.8 s^{-1}. Concentrations after mixing: HEPES, 34 mM (pH 7); DM, 0.01%; ascorbate, 0.45 mM; TMPD, 11 μM; ethylene glycol, 40%; enzyme, 11 μM.

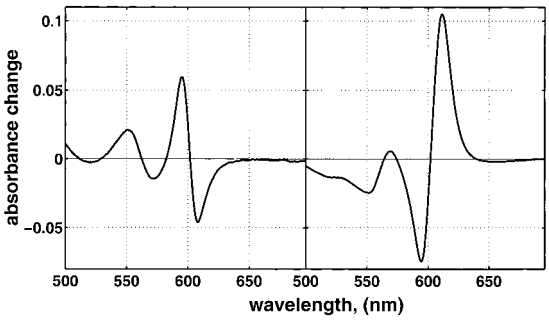

FIGURE 5: Kinetic component spectra from reactions of mixed-valence V279I mutant cytochrome aa_3 from *P. denitrificans* with O_2 at low temperature (−20 °C): left panel, rate constant too fast to resolve accurately; right panel, $k = 7.4$ s^{-1}. Spectra were obtained by a two-component fit; see Materials and Methods. Concentrations after mixing: HEPES, 25 mM (pH 7); DM, 0.03%; ethylene glycol, 40%; enzyme, 11 μM.

followed by an increase in absorbance as oxygen binds to Fe_{a3} to form intermediate **A** ($\tau \sim 7$ μs) and then a decrease as **A** is converted to the $\mathbf{P_R}$ intermediate, simultaneously with oxidation of Fe_a ($\tau \sim 35$ μs). These kinetics are similar to those reported earlier for the bovine enzyme (see Introduction and Figure 1).

In the V279I mutant enzyme, both the rise and the subsequent decrease in absorbance at 595 nm are much slower than in the wild type. The rate of formation of compound **A** has decreased almost 30-fold ($\tau \sim 196$ μs), indicating that the replacement of valine-279 by isoleucine has interfered with binding of oxygen to the heme. However, this cannot be the only effect of the mutation. If the step which follows oxygen binding had its normal rate ($\tau \sim 35$ μs), such slow oxygen binding should go almost unobserved, as is the case when the wild-type enzyme reaction takes place at low oxygen concentrations (*9*, *43*). It follows that the next step after oxygen binding—the conversion of **A** to the $\mathbf{P_R}$ intermediate—has also been significantly retarded in the mutant. This can be seen more clearly at other wavelengths. The center panel of Figure 3 shows flow-flash traces at 605 nm where the dominant contribution to the absorbance change comes from the oxidation of Fe_a. In wild-type enzyme the initial oxidation of this center takes place rapidly ($\tau \sim 35$ μs; see Introduction and Figure 1), but in the V279I mutant, this change is preceded by a significant lag, and the entire process is slow relative to the wild-type enzyme.

The λ_{max} of the **F** intermediate is at 580 nm. At this wavelength, a flow-flash trace for the V279I mutant (right-hand panel of Figure 3) shows a rise and a decay, both phases being significantly slower than would be expected for the wild-type enzyme, based on the similarity between *P. denitrificans* and bovine cytochromes aa_3.

To extend these single wavelength data, the reaction of the enzyme with O_2 was carried out using a low-temperature flow-flash technique which allows the reaction to be followed across the entire spectrum (*21*). Figure 4 shows spectra of the three major kinetic phases in the reaction of the fully reduced V279I mutant enzyme with O_2 at ∼−20 °C, obtained by a global kinetic fit (see Materials and Methods). The fastest component (left panel) indeed reflects the binding of O_2 to the reduced binuclear center to form intermediate **A** (λ_{max} near 595 nm). In the bovine enzyme, this phase was impossible to observe with the 1 ms/spectrum resolution of our instrument (*21*), but it is clearly visible here because the process is much slower in the V279I mutant. The second reaction component (center panel) shows the sum of three simultaneous changes, viz. conversion of intermediate **A** (decreased absorption at 595 nm) to intermediate $\mathbf{P_R}$ (increased absorption at 607 nm), together with net oxidation of a significant portion of Fe_a (decreased absorption at 605 nm; see ref *21*). The third component (right panel) shows the formation of the fully oxidized enzyme, indicated by the appearance of the absorbance band in the 660 nm region. This component reflects the decay of the **F** intermediate at 580 nm, together with the oxidation of the remaining Fe_a (decreased absorption at 605 nm).

The simpler reaction of O_2 with the mixed-valence V279I mutant enzyme was also studied by the low-temperature technique. Figure 5 shows spectra of the two phases of this reaction (see Introduction and Figure 1, right). The first phase (left panel) reflects binding of oxygen and is essentially identical to the first phase of the fully reduced reaction (Figure 4, left panel). The second phase (right panel) shows the conversion of intermediate **A** to intermediate $\mathbf{P_M}$, reflected by a trough near 595 nm and a peak near 610 nm, respectively. Unlike the corresponding phase in the reaction of the fully reduced enzyme (Figure 4, center panel), here there is no oxidation of Fe_a to complicate the spectrum. In the V279I enzyme, under these conditions, this step takes place extremely slowly; the time constant is 135 ms as compared to 4.5 ms in the bovine enzyme at the same temperature (*21*).

Taken together, these data show that the V279I mutation exerts two rather different effects. First, it apparently inhibits the binding of oxygen to Fe_{a3}, and second, it slows down all subsequent processes of reduction of O_2 to water. Investigations of these two aspects of the reaction will be presented in turn.

One reason that the individual steps in reduction of the bound oxygen could be slowed is if the mutation has decreased the rate of the underlying electron-transfer processes, in particular, heme-to-heme electron transfer (see Introduction). However, the low-temperature flow-flash data show that the formation of the **P** intermediate is slower in the V279I mutant than in wild-type enzyme regardless of whether Fe_a is able to contribute an electron to the reaction

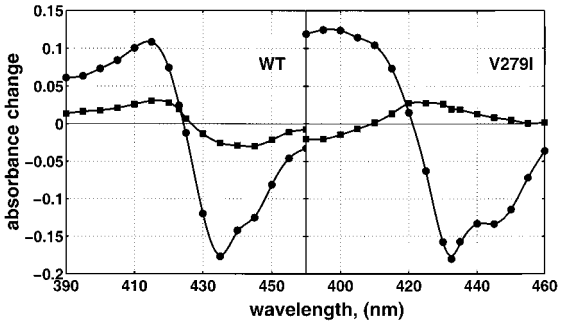

FIGURE 6: Kinetic component spectra of the processes which follow photolysis of CO from CO mixed-valence wild-type and V279I mutant cytochrome aa_3 from *P. denitrificans*: circles, first phase, wild type, $\tau = 3$ μs, V279I, $\tau = 2.5$ μs; squares, second phase, wild type, $\tau = 46$ μs, V279I, $\tau = 10$ μs. Conditions: HEPES, 50 mM, pH 7.0; DM, 0.1%; CO, 1 atm. Spectra were obtained by a two-component fit; see Materials and Methods.

or not. This suggests that the cause for the slow redox reactions is not the heme−heme electron transfer per se. However, the rates of electron transfer between sites in the enzyme can also be studied directly. When CO is photolyzed from the CO mixed-valence form of the enzyme, in the absence of O_2, the redox potential of Fe_{a3} drops, and electrons are free to redistribute to the previously oxidized metal centers, Fe_a and Cu_A. In bovine cytochrome aa_3 two phases of fast electron transfer are observed: The first phase ($\tau \sim 3$ μs) has been assigned as electron transfer from Fe_{a3} to Fe_a (*43*). The second phase ($\tau \sim 35$ μs) consists of electron redistribution out of this $Fe_{a3} \leftrightarrow Fe_a$ equilibrium to Cu_A (*44*). The same processes are found in cytochrome aa_3 from *Rhodobacter sphaeroides*, where the apparent rate constants are almost identical, but the amplitudes of the electron redistributions are different (*45*). We used this method to study internal electron transfer in wild-type and V279I cytochrome aa_3 from *P. denitrificans*. The left panel of Figure 6 shows the results of a two-component global kinetic fit to the data for the wild-type enzyme. The two major phases of absorbance change which take place following photolysis of the wild-type CO mixed-valence enzyme have rates and spectra quite similar to those observed in the bovine (*44*) and *R. sphaeroides* (*45*) enzymes. The faster component may, in fact, be made up of two processes; a three-component model leads to a slightly better fit (not shown). In the wild-type enzyme, the E_m of Fe_a is approximately 18 mV more negative than that of Fe_{a3}, based on the amplitude of the first phase at 445 nm.

The right-hand panel of Figure 6 shows the results of a similar two-component fit to the data for the V279I mutant enzyme. The fast phase of electron transfer appears to take place in much the same way as in the wild type. The rate is similar while the spectrum is slightly different, presumably because the mutation perturbs the spectra of the hemes. The slow phase in the mutant enzyme is distinctly different from that in the wild-type enzyme and has yet to be assigned. However, these results were obtained with the two-electron reduced enzyme, where the amplitude of electron redistribution to Cu_A is small. When the bovine enzyme is reduced further, the amplitude of this phase increases, reaching a maximum when the enzyme has taken up about three electrons (*46*). When the V279I mutant sample was allowed to become further reduced, a phase was observed which had a spectrum and time constant typical of the electron transfer from the hemes to Cu_A (not shown). Failure to see this spectrum at the two-electron reduction level is probably an indication that the redox potentials of the metal centers are slightly altered by the mutation or that the magnitude of redox interactions between the metal centers has been changed.

The similarity of the fast phase data for the mutant and wild-type enzymes confirms the expectation that the heme-to-heme electron transfer process is not itself significantly perturbed by the V279I mutation. Since this is the electron-transfer rate on which the trapping of oxygen in the enzyme depends (*9, 11*), these results confirm that the raised apparent K_M for O_2 in the mutant is not attributable to slow heme-to-heme electron transfer.

Another way to investigate the slow binding of O_2 is to study binding of a similar diatomic ligand, viz. carbon monoxide. Like O_2, CO binds to Fe_{a3}^{2+} in the reduced bimetallic site. The Fe_{a3}−CO bond is photolabile, and when it is broken, CO jumps rapidly to Cu_B. At room temperature, the CO then rapidly equilibrates with the external medium and only returns slowly to the Fe_{a3} by way of Cu_B (*8*). In the wild-type *P. denitrificans* enzyme, CO rebinding after photolysis took place with a time constant of approximately 14 ms ([CO] ~ 1 atm, ~20 °C), while in the V279I mutant recombination was only slightly slower ($\tau \sim 18$ ms). However, as described above, the rate-limiting step in CO rebinding is the final transfer from Cu_B to Fe_{a3}. Since this is a relatively slow step ($\tau \sim 1$ ms; ref *8*), this could mask even relatively large changes in accessibility of Cu_B from the external medium.

At lower temperatures, the CO cannot escape from the oxygen binding site (*47*) and this provides a way to study both the Fe_{a3}−CO and Cu_B−CO structures using FTIR spectroscopy (*48*). Figure 7 shows low-temperature light-minus-dark FTIR spectra of wild-type and V279I mutant enzymes. The stretching frequency of CO bound to Fe_{a3} has changed slightly in the mutant (Figure 7, middle). This vibration of the wild type *Paracoccus* cytochrome *c* oxidase shows two conformers, α (1965 cm^{-1}) and β (1954 cm^{-1}) of which the lower frequency β conformer is more occupied. This pattern is usually observed in the cytochrome *c* oxidases only at low pH (*49*), but here it is observed at pH 8. At higher temperature (278 K) most of the enzyme is in the α conformer (not shown). The V279I mutant enzyme also has two conformers, the frequencies of which are slightly shifted from those of the wild-type enzyme, suggesting small local changes at the binuclear center (Figure 7, middle). This figure also shows that the mutation has a slight effect on the CO stretching vibrations when carbon monoxide is bound to Cu_B.

There are also changes in the vibrational modes assigned to heme a_3 (*50, 51*), most of which are small differences in peak heights. The dominant difference band at 1665 cm^{-1} is an exception (Figure 7; right panel). This signal has been assigned to the $\nu_{C=O}$ of the formyl group of heme a_3 (*50, 52*), although the involvement of other groups, such as amide I and amino acid side chains, cannot be excluded. In the resonance Raman spectrum of the bovine oxidase, this mode is observed at 1665 cm^{-1} in the reduced form and at 1666 cm^{-1} in the reduced CO-bound enzyme (*52*). In the infrared difference spectrum of the bovine enzyme this frequency is shifted from 1660 to 1664.5 cm^{-1} upon photolysis (*50*). In

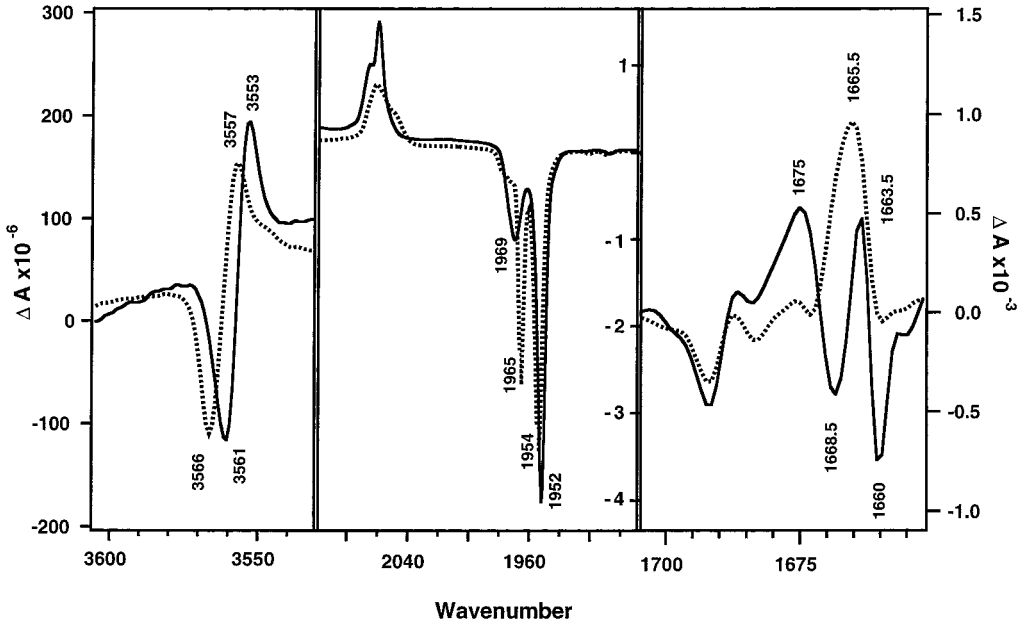

FIGURE 7: Light-minus-dark FTIR spectra of fully reduced, CO-bound cytochrome aa_3: wild type (dashes) and V279I mutant (solid) enzymes. The spectra were normalized using the integrated intensities of the Fe_{a3}−CO peaks. Resolution: 2 cm^{-1}. The center panel shows the CO stretching region for the metal bound CO, the left panel shows the region typical for the asymmetric O−H(D) stretch of hydrogen bonded H_2O (HOD), and the right panel shows the region of the $\nu_{C=O}$ of the formyl group of heme a_3. The spectrum of wild-type enzyme is the result of 3136 scans; the spectrum of the V279I enzyme is the result of 3008 scans. See Materials and Methods.

the *Paracoccus* wild-type enzyme the $\nu_{C=O}$ of the formyl group is not a clear derivative-shaped feature as it is in the bovine enzyme. This could be related to the two separate α and β frequences for the ν_{Fe-CO} vibration, suggesting that the two heme conformers may also be reflected in the formyl vibration. Two corresponding $\nu_{C=O}$ modes may be close to one another, causing the observed broadening of the light-minus-dark difference spectrum (Figure 7, right). In contrast, in the V297I mutant enzyme the two main iron-bound CO modes are 17 cm^{-1} apart. Thus the two observed light/dark shift features at 1675/1668.5 and 1663.5/1660 cm^{-1} could arise from two different formyl surroundings. Finally, a possible ν_{O-H} mode at 3566/3557 cm^{-1} in the difference spectrum is shifted to lower frequency by the mutation (Figure 7, left panel). It is concluded that the structure of the binuclear heme−copper site is somewhat perturbed in the V297I mutant but that the perturbation is relatively small, in agreement with the fact that the V_{max} is decreased only by ~50%.

DISCUSSION

Construction of the V279I mutant in cytochrome aa_3 of *P. denitrificans* has allowed us to use fast kinetics method to probe further into the consequences of replacing this virtually invariant valine near the oxygen binding site by a somewhat bulkier group. Like the corresponding mutant in *E. coli*, this enzyme exhibits a significantly higher apparent K_M for oxygen, which suggests that entry of oxygen into the enzyme is hindered by the mutation (*6*). This view has now been corroborated by flow-flash studies which show that the initial binding of O_2 in this mutant enzyme is much slower than in the wild type. However, it is also clear from the kinetic results that this single point mutation has effects on more than one aspect of the catalytic cycle. If slow oxygen entry were the only consequence of the mutation, we would expect subsequent steps in the reaction to take place at their normal rates. Instead, the reaction step which follows oxygen binding—conversion of intermediate **A** to **P**—is also slow, as are subsequent reaction phases.

The mutation could give rise to slow O_2 binding in at least two ways: First, the larger isoleucine side chain could partially block the putative oxygen channel, restricting O_2 entry into the vicinity of the Fe_{a3}−Cu_B oxygen reduction site. Alternatively, the isoleucine side chain may interfere directly with binding of diatomic ligands to Fe_{a3}. The slightly reduced rate of CO rebinding after photolysis is consistent with both alternatives. Although we cannot exclude that CO diffusion from Cu_B into the medium may be retarded to some extent by the mutation, this cannot be the rate-limiting step in the binding of O_2 since in such a case a lag would have been observed in the kinetics of formation of intermediate **A**, and this is not seen (Figure 3, left panel). Therefore, the effect of the mutation appears primarily to be interference with the binding of a diatomic ligand to Fe_{a3}. In the FTIR spectrum, both the Fe_{a3}−CO and Cu_B−CO peaks are slightly perturbed by the mutation. The perturbed Fe_{a3}−CO vibration is consistent with directly hindered ligand binding, but in other cases perturbations of this signal have been brought about by mutations of amino acid residues which are not in contact with the heme (e.g. ref *49*).

Likewise, there could be several possible explanations for the slow reactions which follow oxygen binding. As described above, if the underlying electron-transfer processes were to be slowed, this would be expected to affect the rate of steps in the oxygen reaction. However, direct measurements of the rates of heme-to-heme and heme-to-Cu_A electron transfer show that neither is significantly affected by the mutation.

Two other possible causes must be considered. First, if, as discussed above, the isoleucine chain were able to interfere with O_2 binding directly, this perturbation might also affect the nature of binding of the oxygen moiety to the heme in a

way that interfers with optimum catalysis of subsequent reaction steps. The fact that the FTIR spectrum shows the Fe_{a3}−CO peak only slightly perturbed weighs against this explanation. Second, the isoleucine could interfere with proton-transfer events. All steps beyond the **P** intermediate require net proton uptake (*53*; Figure 1, left). In addition, whereas no protons are taken up from the solution in the **A** → **P** transition, the rate of formation of **P** shows a solvent deuterium isotope effect of about 1.4 in the reactions of both the fully reduced (*53*) and half-reduced (*54;* M.V., J.E.M., and M.W., unpublished) enzymes with oxygen. EXAFS experiments have suggested that a water molecule is near Cu_B in the reduced binuclear site (*55*), and ab initio density functional calculations (*56*) have indicated that such a water molecule is essential for the O−O bond splitting reaction that forms the **P** intermediate. Moreover, statistical mechanical calculations on the X-ray structural models have suggested that 2−3 water molecules may lie between the conserved glutamic acid 278 and the binuclear site and that one additional water molecule lies at an O−Cu distance of ca. 2.6 Å from Cu_B (*57*, *58*), in agreement with the EXAFS data. Modeling suggests that this latter water molecule may be significantly displaced upon changing the valine 279 to isoleucine, and this may explain the strongly decelerated conversion of intermediate **A** to **P**. The other water molecules modeled in this domain have been suggested to relay protons from the conserved glutamic acid 278 toward the binuclear center (*57*, *58*). Since they are also predicted to lie very close to the side chain of valine 279, the mutation to isoleucine may compromise the formation of such a proton-conducting path. However, the crystal structures have not revealed water molecules in this region of the enzyme. This may be due to their intrinsic mobility, or they may be present to form a transient hydrogen-bonded, proton-conducting pathway only in certain states of the catalytic cycle (*58*). In either case, the formation of such an ordered chain of water molecules may be disturbed by the valine to isoleucine mutation, with the consequence that proton transfer to the binuclear center may be retarded. This would explain the observation that all reaction steps beyond the **P** intermediate are retarded by the mutation.

Most of the present evidence suggests that all those protons that are destined to be pumped across the membrane, as well as many of those to be utilized in water formation in the binuclear site, are transferred via the so-called D-channel, involving the aforementioned conserved glutamic acid 278 (see ref *58*). Hence, a "bifurcation" of proton transfer for pumping or for consumption at the binuclear site would be expected beyond the glutamic acid residue in the channel, whether this occurs by means of a histidine cycle type of mechanism (*59, 60*) or by some other more direct mechanism (*61*). In this respect it may be of interest to note that due to the position of the valine side chain in the structure, relative to the predicted water molecules, its mutation to isoleucine would primarily be expected to retard proton transfer into the binuclear center but not to affect the efficiency of proton translocation, which is consistent with the observations in this work.

In conclusion, we suggest that the mutation of valine 279 to isoleucine has three discrete effects on the function of the enzyme. First, it hinders formation of the oxygen adduct of heme a_3 (compound **A**) by sterically hindering O_2 diffusion into the site and/or proper binding of O_2 to the heme. Second, it may displace a water molecule in the O_2 reaction site (*55*) that is essential in the O−O bond splitting reaction (*56*), thereby decelerating the conversion of intermediate **A** to intermediate **P**. Finally, the isoleucine side chain may prevent proper organization of water molecules that assist proton transfer from glutamic acid 278 into the oxygen reduction site, thereby retarding the reaction steps which convert state $\mathbf{P_R}$ to **F** and **F** to **O**, both of which depend on net proton uptake from the inside of the membrane.

REFERENCES

1. Babcock, G. T., and Wikström, M. (1992) *Nature 356*, 301−309.
2. Wikström, M. (1977) *Nature 266*, 271−273.
3. Tsukihara, T., Aoyoma, H., Yamasita, E., Tomizaki, T., Yamaguchi, H., Shinzawa-Itoh, K., Nakashima, R., Yaono, R., and Yoshikawa, S. (1995) *Science 269*, 1069−1074.
4. Tsukihara, T., Aoyama, H., Yamashita, E., Tomizaki, T., Yamaguchi, H, Shinzawa-Itoh, K., Nakashima, R., Taono, R., and Yoshikawa, S. (1996) *Science 272*, 1136−1144.
5. Iwata, S., Ostermeier, C., Ludwig, B., and Michel, H. (1995) *Nature 376*, 660−669.
6. Riistama, S., Puustinen, A., García-Horsman, A., Iwata, S., Michel, H., and Wikström, M. (1996) *Biochim. Biophys. Acta 1275*, 1−4.
7. Hofacker, I., and Schulten. K. (1998) *Proteins 30*, 100−107.
8. Woodruff, W. H., Einarsdóttir, O., Dyer, R. B., Bagley, K. A., Palmer, G., Atherton, S. J., Goldbeck, R. A., Dawes, T. D., and Kliger, D. S. (1991) *Proc. Natl. Acad. Sci. U.S.A. 88*, 2588−2592.
9. Verkhovsky, M. I., Morgan, J. E., and Wikström, M. (1994) *Biochemistry 33*, 3079−3086.
10. Chance, B., Saronio, C., and Leigh, J. S. (1975) *J. Biol. Chem. 250*, 9226−9237.
11. Verkhovsky, M. I., Morgan, J. E., Puustinen, A., and Wikström, M. (1994) *Nature 380*, 268−270.
12. Wikström, M. (1981) *Proc. Natl. Acad. Sci. U.S.A. 78*, 4051−4054.
13. Hill, B. C., and Greenwood, C. (1984) *Biochem. J. 218*, 913−921.
14. Han, S., Ching, Y. C., and Rousseau, D. L. (1990) *Proc. Natl. Acad. Sci. U.S.A. 87*, 2491−2495.
15. Hill, B. C. (1991) *J. Biol. Chem. 266*, 2219−2226.
16. Hill, B. C. (1994) *J. Biol. Chem. 269*, 2419−2425.
17. Morgan, J. E., Verkhovsky, M. I., Puustinen, A., and Wikström, M. (1993) *Biochemistry 32*, 11413−11418.
18. Svensson, M., and Nilsson, T. (1993) *Biochemistry 32*, 5442−5447.
19. Svensson-Ek, M., Thomas, J. W., Gennis, R. B., Nilsson, T., and Brzezinski, P. (1996) *Biochemistry 35*, 13673−13680.
20. Hill, B. C., and Greenwood, C. (1983) *Biochem. J. 215*, 659−667.
21. Morgan, J. E., Verkhovsky, M. I., and Wikström, M. (1996) *Biochemistry 35*, 12235−12240.
22. Weng, L., and Baker, G. M. (1991) *Biochemistry 30*, 5727−5733.
23. Fabian, M., and Palmer, G. (1995) *Biochemistry 34*, 13802−13810.
24. Wang, J., Rumbley, J., Ching, Y.-c., Takahashi, R. B., Gennis, R. B., and Rousseau, D. L. (1995) *Biochemistry 34*, 15504−15511.
25. Proschlyakov, D. A., Ogura, T., Shinzawa-Itoh, K., Yoshikawa, S., and Kitagawa, T. (1996) *Biochemistry 35*, 76−82.
26. Proschlyakov, D. A., Pressler, M. A., and Babcock, G. T. (1998) *Proc. Natl. Acad. Sci. U.S.A. 95*, 8020−8025.
27. Ostermeier, C., Harrenga, A., Ermler, U., and Michel, H. (1997) *Proc. Natl. Acad. Sci. U.S.A. 94*, 10547−10553.
28. Yoshikawa, S., Shinzawa-Itoh, K., Nakashima, R., Yaono, R., Tamashita, E., Inoue, N., Yao, M., Fei, M. J., Libeu Peters, C., Mizushima, T., Yamaguchi, H., Tomizaki, T., and Tsukihara, T. (1998) *Science 280*, 1723−1729.

29. Buse, G., Soulimane, T., Dewor, M., Meyer, H. E., and Blüggel, M. (1999) *Protein Sci. 8*, 985−990.
30. Varotsis, C., and Babcock, G. T. (1990) *Biochemistry 29*, 7357−7362.
31. Ogura, T., Takahashi, S., Hirota, S., Shinzawa-Itoh, K., Yoshikawa, S., Appleman, E. H., and Kitagawa, T. (1993) *J. Am. Chem. Soc. 115*, 8527−8536.
32. Han, S., Ching, Y. C., and Rousseau, D. L. (1990) *Nature 348*, 89−90.
33. Verkhovsky, M. I., Morgan, J. E., Puustinen, A., and Wikström, M. (1996) *Biochemistry 35*, 16241−16246.
34. Vandeyar, M., Weiner, M., Hutton, C., and Batt, C. (1988) *Gene 65*, 129−133.
35. Raitio, M., Pispa, J. M., Metso, T., and Saraste, M. (1990) *FEBS Lett. 261*, 431−435.
36. Gerhus, E., Steinrücke. P., and Ludwig, B. (1990) *J. Bacteriol. 172*, 2392−2400.
37. De Grier, J. W. L., Lübben, M., Reijnders, W. N. M., Tipker, C. T., Slotbloom, D. J., Van Spanning, R. J. M., Stouthammer, A. J., and Van der Oost, J. (1994) *Mol. Microbiol. 13*, 183−196.
38. Chang, J. P., and Morris, J. G. (1962) *J. Gen. Microbiol. 29*, 301−310.
39. Riistama, S., Laakkonen, L., Wikström, M., Verkhovsky, M. I., and Puustinen, A. (1999) *Biochemistry 38*, 10670−10677.
40. Puustinen, A., Finel, M., Virkki. M., and Wikström, M. (1989) *FEBS Lett. 249*, 163−167.
41. Provincer, S. W., and Vogel, R. H. (1983) Regularization techniques for inverse problems in molecular biology in *Progress in Scientific Computing* (Deuflhard, P., and Hairer, E., Eds.) Vol. 2, pp 304−319, Birkhäuser, Boston, MA.
42. Gibson, Q. H., and Greenwood, C. (1963) *Biochem. J. 86*, 541−555.
43. Oliveberg, M., and Malmström, B. G. (1991) *Biochemistry 30*, 7053−7057.
44. Verkhovsky, M. I., Morgan, J. E., and Wikstrom, M. (1992) *Biochemistry 31*, 11860−11863.
45. Ädelroth, P. Brzezinski, P., and Malmström, B. G. (1995) *Biochemistry 34*, 2844−2849.
46. Jasaitis, A., Verkhovsky, M. I., Morgan, J. E., Verkhovskaya, M. L., and Wikstrom, M. (1999) *Biochemistry 38*, 2697−2706.
47. Sharrock, M., and Yonetani, T. (1976) *Biochim. Biophys. Acta 434*, 333−344.
48. Alben, J. O., Moh. P. P., Fiamingo, F. G., and Altschuld, R. A. (1981) *Proc. Natl. Acad. Sci. U.S.A. 78*, 234−237.
49. Mitchell, D. M., Shapleigh, J. P., Archer, A. M., Alben, J. A., and Gennis, R. B. (1996) *Biochemistry 35*, 9446−9450.
50. Park, S., Pan, L.-P., Chan, S. I., and Alben, J. O. (1996) *Biophys. J. 71*, 1036−1047.
51. Hellwig, P., Grzybek, S., Behr, J., Ludwig, B., Michel, H., and Mäntele, W. (1999) *Biochemistry 38*, 1685−1694.
52. Babcock, G. T. (1988) Raman Scattering by Cytochrome Oxidase and by Heme a Model Compounds in *Biological Applications of Raman Spectroscopy* (Spiro, T. G., Ed.) pp 293−346, John Wiley and Sons, New York.
53. Oliveberg, M., Brzezinski, P., and Malmström, B. G. (1989) *Biochim. Biophys. Acta 977*, 322−328.
54. Karpefors, M., Ädelroth, P., Aagaard, A., Smirnova, I. A., and Brzezinski, P. (1999) *Isr. J. Chem*., in press.
55. Ralle, M., Verkhovskaya, M. L., Morgan, J. E., Verkhovsky, M. I., Wikström, M., and Blackburn, N. J. (1999) *Biochemistry 38*, 7185−7194.
56. Blomberg, M. R. A., Siegbahn, P. E. M., Babcock, G. T., and Wikström, M. (1999) *J. Bioinorg. Chem*., in press.
57. Riistama, S., Hummer, G., Puustinen, A., Dyer, R. B., Woodruff, W. H. and Wikström, M. (1997) *FEBS Lett. 414*, 275−280.
58. Wikström, M. (1998) *Curr. Opin. Struct. Biol. 8*, 480−488.
59. Morgan, J. E., Verkhovsky, M. I., and Wikström, M. (1994) *J. Bioenerg. Biomembr. 26*, 599−608.
60. Wikström, M. (2000) *Biochim. Biophys. Acta*, in press.
61. Michel, H. (1999) *Biochemistry 38*, 15129−15140.

BI000123W